Inter-Research Science Publisher

Marine Ecology Progress Series
Volume 752:51–68

Published January 16, 2025
https://doi.org/10.3354/meps14752

Hydrogen peroxide fluxes and fate in a temperate seagrass ecosystem

Kalina C. Grabb[1,5], Scott D. Wankel[2], Kevin M. Sutherland[3,4], Samuel H. Bowman[2,6], Matthew H. Long[2], Colleen M. Hansel[2,*]

[1]MIT-WHOI Joint Program in Oceanography/Applied Ocean Science & Engineering, Cambridge and Woods Hole, MA 02543, USA
[2]Marine Chemistry and Geochemistry, Woods Hole Oceanographic Institution, Woods Hole, MA 02543, USA
[3]Department of Earth and Planetary Sciences, Harvard University, Cambridge, MA 02138, USA
[4]Isometric, New York, NY 10001, USA

[5]*Present address:* Marine Policy Center, Woods Hole Oceanographic Institution, Woods Hole, MA 02543, USA

[6]*Present address:* Department of Geology and Geography, West Virginia University, Morgantown, WV 26506, USA

ABSTRACT: Seagrass ecosystems rank among the most productive marine environments on the planet, hosting high cycling rates of many globally relevant elements. While the cycling of reactive oxygen species (ROS) has important links with other redox-related biogeochemical cycles (i.e. trace metals, carbon, nitrogen, and oxygen), the dynamics of ROS in seagrass ecosystems are poorly characterized. To assess the flux, decay rate, and fate of ROS, this study quantified rates of hydrogen peroxide (H_2O_2) production and decay through *in situ* incubations of seawater, algae *Polysiphonia* sp., and seagrass *Zostera marina* from a seagrass meadow near Woods Hole, MA, USA. Daytime net primary production values within incubations of *Polysiphonia* and *Zostera* ranged from 12.6 to 137.4 µmol O_2 g dry wt^{-1} h^{-1}. By comparison, hydrogen peroxide dynamics were much more variable, with fluxes ranging from −272 to 150 nmol g dry wt^{-1} h^{-1}, net production rates ranging from −2212 to 38 000 nmol g dry wt^{-1} h^{-1}, and decay rate constants ranging from 0.314 to 9.09 h^{-1}. These results suggest that seagrass meadows contribute to rapid and dynamic turnover of ROS. In separate incubations, tracing of isotopically labeled hydrogen peroxide ($H_2{}^{17}O_2$) indicated that hydrogen peroxide decay was predominantly regulated by peroxidase-like activity (62 to 100%), suggesting that hydrogen peroxide serves primarily as an oxidant of likely various reduced substrates, which were not identified here. This study documents the rapid cycling and reductive decay pathways of hydrogen peroxide within seagrass ecosystems, laying the foundation for future studies of ROS cycling dynamics in these and other related shallow marine ecosystems.

KEY WORDS: Hydrogen peroxide · Seagrasses · Redox · Biogeochemistry · Reactive oxygen species

1. INTRODUCTION

Seagrass meadows are highly productive coastal environments (Duarte & Chiscano 1999) that are distributed across the globe (Orth et al. 2006) and provide essential ecosystem services, including oxygen production, carbon sequestration (~20–100 Tg C yr^{-1} globally), and coastal protection (Duarte et al. 2010, Kuwae & Hori 2019, Novak et al. 2020). Although seagrasses are vital to maintaining healthy coastal environments, they are currently experiencing rapid loss (globally 7% per year areal extent decrease), warranting urgent ecosystem restoration and investigation into controls on their health and ecological function (Jordà et al. 2012, Valdez et al. 2020). While seagrass ecosystems are comprised of a resilient array of pho-

*Corresponding author: chansel@whoi.edu

Publisher: Inter-Research · www.int-res.com

tosynthetic macrophytes (e.g. seagrasses, macroalgae, microalgae, etc.) as well as corals, ecosystem degradation is likely to increase with anthropogenic stressors (i.e. sea-level rise, increased turbidity, elevated nutrient inputs, higher temperatures, etc.). This can alter light levels and ecosystem composition of these coastal environments, having compounding effects on productivity and biogeochemical processes (Short et al. 2011, Waycott et al. 2019). Thus, it is valuable to understand the relative roles of different macrophytes in seagrass meadow ecosystems and their links with various biogeochemical cycles (e.g. oxygen, carbon, metals, nutrients, etc.). Among these actively hosted biogeochemical cycles, reactive oxygen species (ROS) play important roles in many biogeochemical reactions in marine ecosystems, and their dynamics have been shown to vary across different environmental conditions and organisms (see Hansel & Diaz 2021 and references within). Nevertheless, ROS dynamics associated with seagrass systems remain largely unstudied.

Given the high irradiance levels, abundance of productive photosynthetic biomass, and elevated influxes of metals, nutrients, and chromophoric dissolved organic matter (CDOM) found in seagrass ecosystems (Stabenau et al. 2004), seagrass ecosystems may be especially conducive to high fluxes of ROS, leading to a cascade of redox reactions that can influence other elemental cycles. ROS are short-lived oxygen-containing intermediates that include superoxide (O_2^-; half-life ~seconds to minutes) and hydrogen peroxide (H_2O_2; half-life ~minutes to hours) (Petasne & Zika 1997, Fridovich 1998). Although superoxide cannot pass through intact biological membranes, hydrogen peroxide is membrane-permeable, allowing intracellular production to contribute to extracellular pools and fluxes (Korshunov & Imlay 2002, Diaz et al. 2013, Armoza-Zvuloni & Shaked 2014). Intracellular and extracellular superoxide and hydrogen peroxide are often produced as byproducts of major metabolic reactions (i.e. photosynthesis and respiration) as well as through a series of biotic and abiotic processes mediated by a wide range of organisms, including fungi, bacteria, plankton, and larger eukaryotes (Rose et al. 2008, Diaz et al. 2013, Grabb et al. 2019, Sutherland et al. 2019, Bond et al. 2020). Specifically, ROS can be produced extracellularly via transmembrane, outer membrane-bound, or soluble extracellular enzymes, such as NAD(P)H oxidoreductase enzymes, heme peroxidases, and/or glutathione reductases (GR) (Diaz et al. 2013, 2019, Andeer et al. 2015). Abiotic photochemical reactions and dark (light-independent) reactions are also major environmental sources of ROS, including reactions with dissolved redox-active metals (e.g. copper, manganese, iron) and organic matter (Kieber et al. 2003, Heller & Croot 2010, Wuttig et al. 2013).

The fate of H_2O_2 can be controlled by enzymatic activity as well as (photo)chemical processes, both of which can degrade hydrogen peroxide to molecular oxygen (O_2) and/or water (H_2O). It is thought that microbially mediated enzymatic decomposition of hydrogen peroxide is driven by a suite of enzymes, mainly catalase and peroxidase enzymes (Cooper & Zepp 1990, Moffett & Zafiriou 1990, 1993). Within *Zostera* and *Polysiphonia*, catalases, peroxidases, and other enzymatic processes (e.g. the ascorbate-glutathione cycle and superoxide dismutase, SOD, which dismutates superoxide to produce hydrogen peroxide and oxygen) have been found to alter hydrogen peroxide concentrations and decay rates, varying with environmental (e.g. temperature, oxygen, and metal concentrations; Lin et al. 2016, Liu et al. 2016, Zang et al. 2018, Greco et al. 2019, Zhang et al. 2021, Pei et al. 2024, Yan et al. 2024) and intracellular (e.g. H_2O_2 and ascorbic acid concentrations; Dummermuth et al. 2003) conditions. Although thought to be a less significant decay flux compared to microbial processes (Moffett & Zafiriou 1993), hydrogen peroxide can also be degraded through both oxidation and reduction reactions with trace elements (e.g. copper, manganese, iron) (Moffett & Zika 1987, Millero & Sotolongo 1989, Hansel 2017), organic matter (CDOM, dissolved organic carbon [DOC]) (Kieber & Blough 1990, Lester et al. 2013, Wuttig et al. 2013), and other nitrogen-, phosphorus- and oxygen-bearing compounds (Sutherland et al. 2020, 2021).

Catalases and peroxidases have distinct hydrogen peroxide degradation stoichiometries that are consistent across a wide range of diverse enzymes. Catalase dismutates hydrogen peroxide to water and molecular oxygen (in a 1:1 ratio), while peroxidases reduce hydrogen peroxide solely to water (Zamocky et al. 2008). It is noteworthy that redox decay pathways can also act with similar stoichiometries as the microbially mediated processes (Dole et al. 1952). Therefore, rather than identifying the exact degradation mechanism, hydrogen peroxide decay pathways are often classified with regards to the stoichiometries of these reactions (Zamocky et al. 2008, Sutherland et al. 2021), as follows:

$$2H_2O_2 \rightarrow 2H_2O + O_2 \text{ (catalase-like)} \quad (1)$$

$$H_2O_2 + AH_2 \rightarrow 2H_2O + A \text{ (peroxidase-like)} \quad (2)$$

where AH_2 is a hydrogen- and electron-donor molecule. The production of hydrogen peroxide and subsequent decay can be determined within a system by tracing the addition of isotopically labeled H_2O_2 (Moffett & Zafiriou 1990, 1993, Sutherland et al. 2021). Using this approach, these prior studies have demonstrated that catalase-like stoichiometric processes were dominant in open ocean waters, suggesting that H_2O_2 was equally lost through oxidative and reductive pathways, with oxidative pathways returning about half of the H_2O_2 to O_2.

Through these degradation pathways, hydrogen peroxide can directly (e.g. through redox reactions) and indirectly (e.g. through the microbial loop) influence the environmental redox capacity and speciation of other compounds (Rose et al. 2008, Wuttig et al. 2013, Twigg et al. 2020). For example, hydrogen peroxide can oxidize Fe(II) (Fenton reaction) to form the hydroxyl radical ($OH^{\bullet}$) and oxidized forms of iron (i.e. Fe(III)), which also decreases the bioavailability of iron by forming oxidized iron compounds that often precipitate, such as ferric hydroxide (Koppenol 1993, Illés et al. 2019). The production of hydroxyl radicals can alter the speciation of other elements, such as bromine and carbon (Zafiriou 1990, Illés et al. 2019). Additionally, reactions between hydrogen peroxide and manganese (Mn) can influence Mn speciation and bioavailability by reducing Mn(IV)oxide forming Mn(III), which is rapidly oxidized through a pathway that also produces O_2 (Do et al. 2009, Hansel 2017, Jones et al. 2020, Zhang et al. 2021). The fate of hydrogen peroxide can also have a direct bearing on the O_2 cycle, with estimates of light-independent biological ROS production and cycling responsible for as much as 19% of the global marine oxygen sink (Sutherland et al. 2020). Within seagrass ecosystems, H_2O_2 cycling is likely intertwined with haloperoxidase activity and other compounds with anti-oxidant properties, such as bromophenolic compounds and polyphenols, which are known to be produced by seagrass species and macroalgae (Achamlale et al. 2009, Piao et al. 2012, Weinberg et al. 2013, Cho et al. 2019, Satoh et al. 2019). Given that previous studies have lacked quantitative measures to classify hydrogen peroxide decay pathways within seagrass ecosystems, characterizing and quantifying the decay and fate of hydrogen peroxide is important to understand its potential as a redox mediator.

The goal of this study was to characterize and quantify hydrogen peroxide production and decay dynamics in relation to oxygen cycling within a seagrass meadow. We isolated the individual contributions of predominant members of the seagrass ecosystem by using individual incubations, which uniquely enabled us to quantify the hydrogen peroxide decay rates and decay pathways. We conducted *in situ* incubations of red algae *Polysiphonia* sp. and seagrass *Z. marina* and measured the fate of hydrogen peroxide by conducting a subset of incubations using $H_2{}^{17}O_2$. Overall, this study highlights the need to understand individual components of the ecosystem to characterize the biogeochemical dynamics and predict how the biogeochemistry of seagrass meadows may respond to future changes in climate.

2. MATERIALS AND METHODS

2.1. Sampling location and timeframe

In situ incubations (Fig. 1) were conducted in seagrass beds on the eastern side of Uncatena Island (41.517426° N, 70.701574° W), located southwest of Woods Hole, MA, USA (Fig. S1 in the Supplement at www.int-res.com/articles/suppl/m752p051_supp.pdf). Three sampling campaigns were conducted in 2021 capturing the beginning, middle, and end of the summer season (June, July, and September). During each campaign, incubations for measuring O_2 and H_2O_2 concentrations and fluxes were conducted over 1 d (for rate measurements, Fig. 1E), and incubations for measuring hydrogen peroxide decay pathways (using ^{17}O tracer, Fig. 1F) were conducted over an additional 1 to 2 d. All daytime incubations started at 09:00 h and were sampled over a ~5 h period to capture photosynthetic activity at the onset and into peak irradiance. To minimize bottle effects within the incubations, the total duration was kept to ~5 h, they were not filled with biomass to capacity to keep the biomass-to-seawater ratio low, and they were placed directly in the seagrass ecosystem to incubate under natural environmental conditions. Following the daytime incubations during the September sampling event, additional incubations were also conducted after sunset, starting at 19:00 h and sampled over ~4 h. Due to constraints in accessing the site via boat, weather conditions, and limitations in time and personnel, evening sampling was restricted to September.

2.2. Seagrass ecosystem characteristics

Throughout the summer, seagrass blade length, seagrass biomass, and algae biomass were quanti-

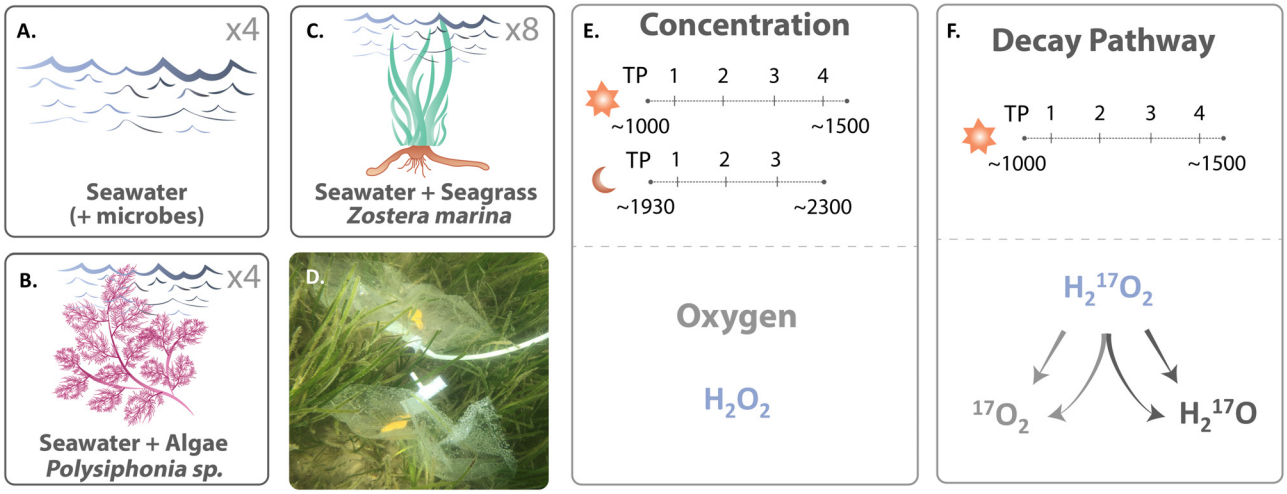

Fig. 1. Schematic of the incubation set-up, with treatments for (A) seawater control, (B) seawater plus *Polysiphonia*, and (C) seawater plus *Zostera*. The number of replicates is indicated in the upper right-hand corner. (D) *Zostera* was incubated intact in the ground, while seawater control and *Polysiphonia* incubations were contained in a milk crate (not shown) at a similar depth as the *Zostera* (~2 m). (E,F) Sampling duration, time points (TP), and analysis for both (E) concentration (µmol for oxygen and nmol for H_2O_2) and (F) decay pathway (used to calculate decay rate constants, k_{loss}, h^{-1}) incubations

fied to characterize the composition of the ecosystem and have been reported elsewhere (Coogan & Long 2023, Text S1). Seawater conditions (Table S1) were monitored hourly for pH, dissolved oxygen, salinity, and temperature using a YSI 556 MPS (YSI Inc.). Photosynthetically active radiation (PAR) was also measured using a LI-1500 PAR Sensor (LI-COR Inc.).

2.3. Seagrass and algae species and biomass

In situ incubations included a seawater-only condition (used to derive the discrete influence of the photosynthetic macrophytes by subtraction), as well as seawater with the addition of red algae *Polysiphonia* sp. or seagrass *Zostera marina* (herein referred to as seawater control, *Polysiphonia*, and *Zostera* incubations, respectively) (Fig. 1A–C). All organisms were collected from the same seagrass ecosystem with the same seawater and environmental conditions (i.e. nutrients, microbial, environmental conditions, etc.), and the control incubations contained all components naturally found in seawater (i.e. microbes, phytoplankton, small zooplankton, etc.). Four (for seawater control and *Polysiphonia* incubations) or 8 (for *Zostera* incubations) biological replicates were conducted for each treatment, and data are presented with the average and standard deviation of these replicates. After each incubation, epiphytes were scraped from the *Zostera*, and the dry weight of the epiphytes, *Polysiphonia*, and *Zostera* biomass was measured using the methods described in Text S1 for normalizing rate measurements to dry biomass (e.g. mol g^{-1} dry wt; Text S1). The dry weight of the epiphytes was not significant compared to the *Zostera* biomass and therefore was not included in the *Zostera* biomass calculations, even though the epiphytes were left intact during the *Zostera* incubations. Seawater control incubations were normalized by volume (e.g. mol l^{-1}).

2.4. Seagrass incubations

In situ incubations were set up using 3 l clear Tedlar bags with one corner cut off for filling the incubations. The Tedlar bags were evaluated for UV absorption, which indicated sunlight transmission of 64–88% (average 72% for wavelengths between 400 and 800 nm) (Fig. S2). This ~25% decrease in sunlight transmission was uniform across all incubations and is within the range of daily fluctuations (10–80% depending on cloud cover) observed across the experimental days (Table S1), providing a conservative estimate of production. Each bag contained an integrated plastic sampling port allowing sampling through a valve-operated outlet tube. For seawater control incubations, 1 l (for concentration/flux incubations) or 500 ml (for decay pathway incubations) of seawater was collected from the site, placed in

the bags, squeezed to remove any air bubbles, sealed, and placed at seagrass depth (~1 m). For the *Polysiphonia* incubations, biomass was collected near the seagrass meadow and added to incubation bags using the same method. For *Zostera* incubations, a plastic stake was screwed into the sediment next to the seagrass shoots (Fig. 1D). One liter of seawater was then placed inside each Tedlar bag and held closed as 1 to 3 seagrass shoots were slipped into the incubation bag underwater and secured to the stake using foam padding and cable tie. This method allowed the seagrass to remain intact in the ground and protected the seagrass from damage. Testing of this approach indicated minimal water exchange and no impact on ROS cycling. All incubation bags were rinsed with seawater prior to each incubation and all sampling materials were tested in previous incubations to assess for contaminants that could influence the ROS cycling, such as trace metals. It is noted that only the above-ground biomass was included in the seagrass incubations and therefore results in this study do not capture processes that may have occurred within the sediments and rhizosphere of the seagrass.

2.5. Concentration measurements

2.5.1. Sample collection

Incubations were sampled initially and every ~60 min over a ~5 h incubation period for oxygen and hydrogen peroxide concentrations. At each sampling timepoint, a 50 ml plastic syringe was used to extract sample water from the incubation sampling port. The syringe was promptly capped, stored in the dark, and processed for concentration measurements (described below) within 20 min. This method ensured no air was introduced to the incubation and minimized chemical alteration prior to processing.

2.5.2. Oxygen fluxes and net primary production

To measure O_2 concentrations, 10 ml of the sample from the collected 50 ml syringe was gently transferred to a 15 ml centrifuge tube and promptly analyzed with a FireSting GO_2 field oxygen meter (PyroScience GmbH). The specific fluxes of *Polysiphonia* and *Zostera* were seawater-corrected and biomass-normalized (see Texts S1 & S2 for additional details). Accounting for the difference between daytime ($flux_{O2}$, net oxygen flux including both photosynthesis and respiration) and evening respiration from September (R, net oxygen flux in the absence of photosynthesis), we determine oxygen net primary production (NPP) (Duarte et al. 2010) as:

$$NPP = flux_{O_2} + R \quad (3)$$

where respiration rates (R) are typically negative values. Areal NPP fluxes (mmol m^{-2} d^{-1}) for *Polysiphonia* and *Zostera* were calculated by multiplying the biomass normalized flux (µmol g dry wt^{-1} hr^{-1}) by biomass density per square meter (g dry wt m^{-2}) in the local ecosystem (data presented in Section 3). While respiration rates associated with *Z. marina* have been observed to be variable throughout the diel cycle (Rasmusson et al. 2017), additional O_2 loss pathways are likely to be elevated during the day compared to the evening (i.e. photorespiration, photoreduction, and/or increases in metabolisms, and therefore cellular respiration) (Badger et al. 2000, Eisenhut et al. 2008). However, quantifying the contributions of these pathways within seagrasses requires additional research (Larkum et al. 2006). Since these NPP measurements do not include oxygen consumption in the sediment and roots, these NPP rates likely lie somewhere between gross primary production (GPP) and NPP rates measured from *Z. marina* within other studies (Jensen et al. 2005, Rasmusson et al. 2017, Peyer et al. 2020, Celebi-Ergin et al. 2022, Brodersen & Kühl 2023). Therefore, this estimation of NPP is a conservative estimate if considering the additional respiration processes, yet is an overestimate if considering the lack of sediment processes, and could also vary seasonally since it is only based on the respiration rates available from September.

2.5.3. Hydrogen peroxide concentration

Hydrogen peroxide concentration was measured using the POHPPA (4-hydroxyphenylacetic acid) technique and associated protocols (Miller et al. 2005, Shaked & Armoza-Zvuloni 2013, Sutherland et al. 2021; see Text S3 for more details). At each time point, samples were collected and analyzed in triplicate alongside a suite of standards (10 nM to 1 µM H_2O_2, see Text S3 for more details) and a blank. Similar to many enzyme-based peroxide methods, this method does not distinguish between hydrogen peroxide and organic peroxide present within the water samples, yet previous testing with this method in a coastal

lagoon indicated that organic peroxides were an insignificant fraction of the total peroxide pool (Shaked & Armoza-Zvuloni 2013). For simplicity, we refer to these measurements as hydrogen peroxide concentrations.

Hydrogen peroxide decay rate constants were calculated using 2 methods, the POHPPA method as described in Texts S3 & S4, and the isotopic method described below. Note that all calculations below involving hydrogen peroxide decay rate constants use those derived by the isotopic method, since it captured decay deriving from *in situ* incubation conditions, and decay rate constants estimated using the POHPPA method are only presented for comparison.

Hydrogen peroxide fluxes ($flux_{H_2O_2}$, nmol g dry wt^{-1} h^{-1}) for the *Polysiphonia* and *Zostera* incubations were seawater-corrected and biomass-normalized in a similar fashion to the calculation of oxygen flux as described in Texts S2 & S3. Briefly, $flux_{H_2O_2}$ was calculated by first taking the slope of change in hydrogen peroxide concentration across time (nmol l^{-1} h^{-1}) for all replicates in the seawater control, *Polysiphonia*, and *Zostera* incubations. Net hydrogen peroxide production rate ($NP_{H_2O_2}$, nmol l^{-1} h^{-1}) was calculated for each incubation using the $flux_{H_2O_2}$ (nmol l^{-1} h^{-1}), the concentration at each time point ($[H_2O_2]_{(t)}$, nmol l^{-1}), and the isotope method-derived decay rate constant (calculated below, $k_{loss,isotope}$, units of h^{-1}) with the following equation:

$$\frac{d\left(NP_{H_2O_2}\right)}{dt} = flux_{H_2O_2} + \left(\left[H_2O_2\right]_{(t)} \times k_{loss,isotope}\right) \quad (4)$$

Hydrogen peroxide flux and net production within *Polysiphonia* and *Zostera* incubations were calculated by subtracting the respective hydrogen peroxide flux and net production from the seawater controls. The flux and net production associated with *Polysiphonia* and *Zostera* were then biomass-normalized using the dry weight (nmol g dry wt^{-1} h^{-1}). Flux and net production associated with the seawater control were normalized to volume of seawater (nmol l^{-1} h^{-1}). For example, *Zostera* flux ($flux_{H_2O_2,Zostera}$) was calculated using the following equation:

$$flux_{H_2O_2,Zostera} = \frac{flux_{H_2O_2,Zostera+\text{Seawater}} - flux_{H_2O_2,\text{Seawater Control}}}{\text{dry weight}_{Zostera}} \quad (5)$$

Areal net production for hydrogen peroxide within all incubations was calculated using the same methods as the oxygen areal NPP calculations (see Text S2 for additional details) to obtain daily areal net hydrogen peroxide production (mmol m^{-2} d^{-1}).

2.6. Isotope measurements

2.6.1. Isotopically labeled $H_2{}^{17}O_2$ incubations

Hydrogen peroxide oxidation rate constants (k_{ox}), reduction rate constants (k_{red}), and the sum of the two (total decay rate constants, $k_{loss,isotope}$) were quantified with the addition of a 500 nM isotopically labeled $H_2{}^{17}O_2$ spike, similar to previous protocols (Moffett & Zafiriou 1990, Sutherland et al. 2021). The concentration of spike was based on these previous studies and was tested to optimize a high enough spike to measure the decay rate and detect the isotopic composition while remaining below 2× the highest hydrogen peroxide starting concentration within the seawater control incubations (monthly average between 60.3 ± 34.3 and 369.6 ± 71.6 nM in September). This method is the most appropriate for all subsequent calculations and analysis because these estimates derive directly from incubations under natural environmental conditions (temperature and sunlight) and with the selected phototrophs. Use of the $H_2{}^{17}O_2$ label (in contrast to a more common ^{18}O label) was chosen for the ease of quantification of derived O_2 using a standard triple collector on an isotope ratio mass spectrometer tuned to mass:charge ratios of 32, 33, and 34 (described further in Sutherland et al. 2021). This ^{17}O label concentration was chosen because it was similar to the highest ambient hydrogen peroxide concentration observed within the seagrass ecosystem, and provided enough hydrogen peroxide to measure and model decay rate constants; however, additional spike concentrations remain to be tested to further determine concentration-dependent effects. In brief, the evolution of doubly ^{17}O substituted $^{34}O_2$ was monitored as it was transformed from the H_2O_2 pool into the dissolved O_2 pool. Mass balance equations were used to quantify the total oxidative and reductive sinks of hydrogen peroxide. To prepare the 500 nM spike with the appropriate isotopic composition, an aliquot of $H_2{}^{17}O_2$ (Berry and Associates/ICON Isotopes) was diluted with 3% H_2O_2 (Sigma) and ultrapure water prior to addition to any incubations. The spike was then added to several liters of seawater, homogenized, and then allocated (500 ml) into replicate incubations with seawater and the respective macrophytes (*Polysiphonia* and *Zostera*). The incubations were squeezed to remove headspace, incubated *in situ* at seagrass depth (~2 m) for ~5 h, and sampled at 3 timepoints. At each timepoint, biological replicates were sacrificially sampled, and dissolved oxygen isotope composition was measured using 2 different analyses (Analysis 1 and Analysis 2), each in

duplicate, following a previous protocol (Sutherland et al. 2021). In brief, Analysis 1 (analogous to Treatment 1 in Sutherland et al. 2021) measured the $^{34}O_2$ (^{17}O-^{17}O) in the dissolved oxygen pool (plus ambient O_2) that resulted from natural $H_2{}^{17}O_2$ oxidation. Analysis 2 (analogous to Treatment 2 in Sutherland et al. 2021) measured the $^{34}O_2$ (^{17}O-^{17}O) in the dissolved oxygen pool (plus ambient O_2) that resulted from both the natural oxidation of $H_2{}^{17}O_2$ and the unreacted $H_2{}^{17}O_2$ by oxidizing the remaining $H_2{}^{17}O_2$ into the ambient oxygen pool through the addition of 4 ml potassium permanganate ($KMnO_4$) (40 mg ml^{-1}) and 400 µl 6 N hydrochloric acid (HCl). No significant changes in O_2 isotopic composition or O_2:Ar ratio were observed in samples regardless of equilibration time, indicating that the approach was robust to atmospheric O_2 contamination. The difference between the 2 analyses was used to calculate the amount of $H_2{}^{17}O_2$ that was remaining, which was used to calculate how much hydrogen peroxide had already been reduced to water (Sutherland et al. 2021). The oxygen isotope composition and O_2:Ar ratio were simultaneously measured on an Isoprime100 isotope ratio mass spectrometer with a manual injection port and recorded as the $\delta^{18}O$ equivalent ($\delta^{18}O' = (^{18}R_{sample}/^{18}R_{standard} - 1) \times 1000$, $R = {}^{18}O/{}^{16}O$), as described previously (Long et al. 2020, Sutherland et al. 2021) (see Text S4). Production of ^{17}O-^{17}O (from H_2O_2) was corrected for photosynthetically produced O_2, which contributes O_2 having a low 18/16 ratio to the native O_2 pool, as follows. Net oxygen production from photosynthesis was estimated from concurrent O_2:Ar values elevated above atmospheric equilibrium and were assumed to have a $\delta^{18}O$ value of ~0‰ (Tcherkez & Farquhar 2007). This derived amount of net oxygen production was then subtracted from the $\delta^{18}O$ measurement to yield corrected levels of ^{17}O-^{17}O production (reported as $\delta^{18}O'$; Text S4).

2.6.2. Hydrogen peroxide decay and production dynamics

The decay of hydrogen peroxide follows pseudo first-order decay kinetics, which we calculate from the change in isotope ratios over time, based on previous methods (Moffett & Zafiriou 1990, Sutherland et al. 2021). Briefly, the fraction (X) of labeled $H_2{}^{17}O_2$ removed was calculated at each time point and used to determine the decay rate constant, with Analysis 1 (A_1) corresponding to the oxidation loss pathway and Analysis 2 (A_2) corresponding to the reduction loss pathway. The following equations demonstrate these calculations:

$$^{34}R = \frac{^{34}O_2}{^{32}O_2} \quad (6)$$

$$X_{label} = \frac{^{34}R_{sample} - {}^{34}R_{no\ spike,\ t=0}}{^{34}R_{A_2,\ t=0} - {}^{34}R_{no\ spike,\ t=0}} \quad (7)$$

where $^{34}R_{no\ spike,\ t\ =\ 0}$ is the isotope ratio at the beginning of an incubation with no isotope label added, and X_{label} corresponds to the fraction of hydrogen peroxide present in the dissolved pool in either Analysis 1 or 2 at any given time point. Finally, both oxidative (k_{ox}) and reductive (k_{red}) decay rates and the total hydrogen peroxide loss (k_{loss}, where $k_{ox} + k_{red} = k_{loss}$) were calculated following Eqs. (8) & (9), based on Sutherland et al. (2021):

$$\left[\frac{d[H_2O_2]}{dt}\right]_{oxidation} = -k_{ox}\left[1 - \left(X_{label}(t)_{Analysis\,1}\right)\right] \quad (8)$$

$$\left[\frac{d[H_2O_2]}{dt}\right]_{reduction} = -k_{red}\left[1 - \left(X_{label}(t)_{Analysis\,2}\right)\right] \quad (9)$$

2.6.3. Statistical analysis and data reporting

Results were analyzed for significance using either a single-factor ANOVA or a 1-tailed *t*-test. Single-factor ANOVA tests were used to investigate differences in fluxes across sampling campaigns, whereas 1-tailed *t*-tests were used to determine if *Polysiphonia* and *Zostera* fluxes were statistically different than the seawater control. For ANOVA, assumption of normality of variance was tested for. Significant variation is defined by p-values < 0.05. Correlation between variables was calculated by linear regression and the coefficient of determination (R^2), where $R^2 > 0.63$ indicates correlation. All reported error values are presented as the average ± SD.

3. RESULTS

3.1. Seagrass ecosystem conditions

Over the summer, *Zostera* blade length increased and was the dominant biomass present compared to *Polysiphonia* and epiphytes (Coogan & Long 2023, Text S1). Continuous monitoring of the seagrass meadow showed that temperature and dissolved oxygen within the meadow waters increased over the summer, likely reflecting higher productivity (or possibly slower gas exchange) during the July and September sampling periods than in June (Coogan &

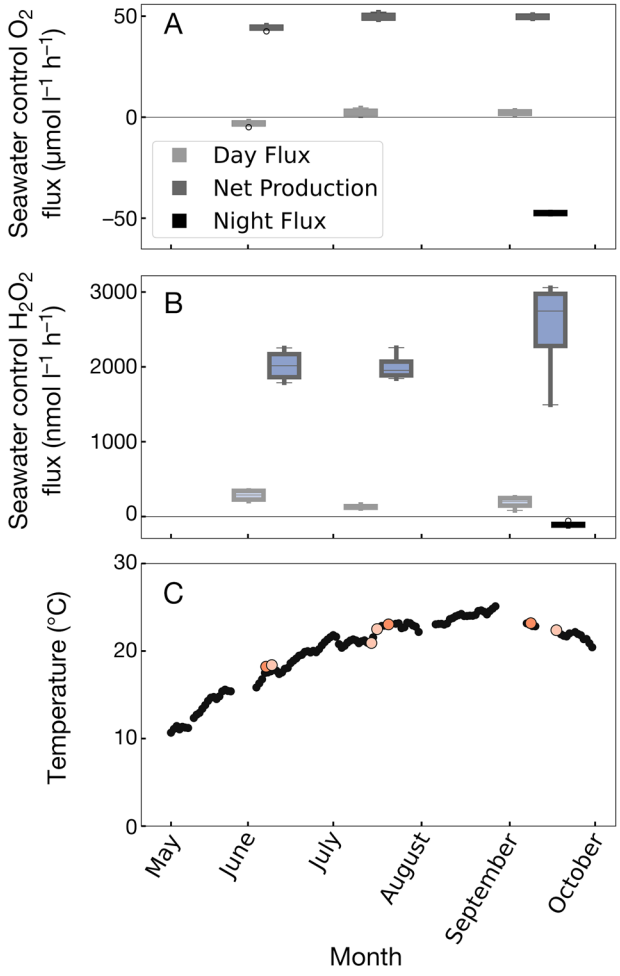

Fig. 2. (A) O_2 and (B) H_2O_2 flux within seawater control incubations across all 3 sample periods (June, July, and September). Boxplots: data from biological replicates, with the middle 50th percentile (box), median (horizontal line), middle 90th percentile (vertical lines), and outliers (open circles). Day fluxes (gray outline, light gray fill) and net production (dark gray outline, blue fill) shown for June, July, and September. Night fluxes (black outline) were only measured in September. (C) Daily average water temperature within the seagrass ecosystem (black circles); dark and light orange circles: measurements on concentration and decay incubation days, respectively (adapted from Coogan & Long 2023)

Long 2023; temperature data shown in our Fig. 2C, Text S1).

3.2. Incubation chemical measurements

3.2.1. Seawater control oxygen and hydrogen peroxide fluxes

Incubations of the seawater controls showed positive fluxes and net production for both oxygen and hydrogen peroxide for nearly all months (except for daytime oxygen flux during June, which is negative) (Fig. 2A, see Table S2 for all oxygen and hydrogen peroxide flux data). The oxygen flux was significantly different across all months (ANOVA $p < 0.001$, Table S3) ranging from −3.2 ± 1.1 (June) to 2.4 ± 1.4 (July) µmol l^{-1} h^{-1}, with June contributing to the most variability as the only negative flux. Oxygen respiration rates within the seawater control were −47.5 ± 0.5 µmol l^{-1} h^{-1}, yielding oxygen NPP from the seawater controls ranging from −44.3 ± 1.1 in June to −49.9 ± 1.4 µmol l^{-1} h^{-1} in July (Fig. 2A). Areal oxygen NPP was very low in June (−93.9 ± 33.1 mmol m^{-2} d^{-1}) and then increased in July and September (74.0 ± 42.6 and 61.5 ± 20.7 mmol m^{-2} d^{-1}, respectively) (see Fig. 4A).

Hydrogen peroxide fluxes in seawater control incubations were only statistically different between June and July (ANOVA $p = 0.008$, Table S3), ranging between 131 ± 20 (July) and 282 ± 64 (June) nmol l^{-1} h^{-1} (Fig. 2B). $NP_{H_2O_2}$ within the seawater control incubations ranged from 2002 ± 158 (July) to 2510 ± 618 (September) nmol l^{-1} h^{-1} (Fig. 2B). Areal net hydrogen peroxide production was similar to areal net oxygen production and varied between the narrow range of 60.1 ± 4.8 mmol m^{-2} d^{-1} (July) and 65.3 ± 16.1 mmol m^{-2} d^{-1} (September) (see Fig. 4B).

3.2.2. *Polysiphonia* and *Zostera* oxygen and hydrogen peroxide fluxes

Biomass-normalized oxygen fluxes and NPP (see Eq. 3) from incubations of *Polysiphonia* and *Zostera* exhibited significant daytime oxygen production by photosynthesis (between 2.5 ± 3.6 and 107.5 ± 72.8 µmol g dry wt^{-1} h^{-1}) and nighttime respiration (between 10.1 ± 2.2 and 29.9 ± 9.4 µmol g dry wt^{-1} h^{-1}) compared to background seawater (*t*-test $p = 0.018$ and <0.001 for *Polysiphonia* and *Zostera*, respectively) (Fig. 3A,B, see Table S2 for oxygen data). All oxygen fluxes, NPP (ranging between 14.4 ± 3.1 and 137.4 ± 72.8 µmol g dry wt^{-1} h^{-1} for all *Polysiphonia* and *Zostera* incubations, Fig. 3A,B), and areal NPP (ranging between 1.3 ± 1.8 and 58.2 ± 39.4 mmol m^{-2} d^{-1} for all *Polysiphonia* and *Zostera* incubations, Fig. 4C) values were higher within *Zostera* incubations compared to *Polysiphonia* for each respective month and most elevated during September. The higher NPP values associated with *Zostera* are expected, since only above-ground biomass was assessed, and thus our approach excluded any respiration that may be occurring below ground.

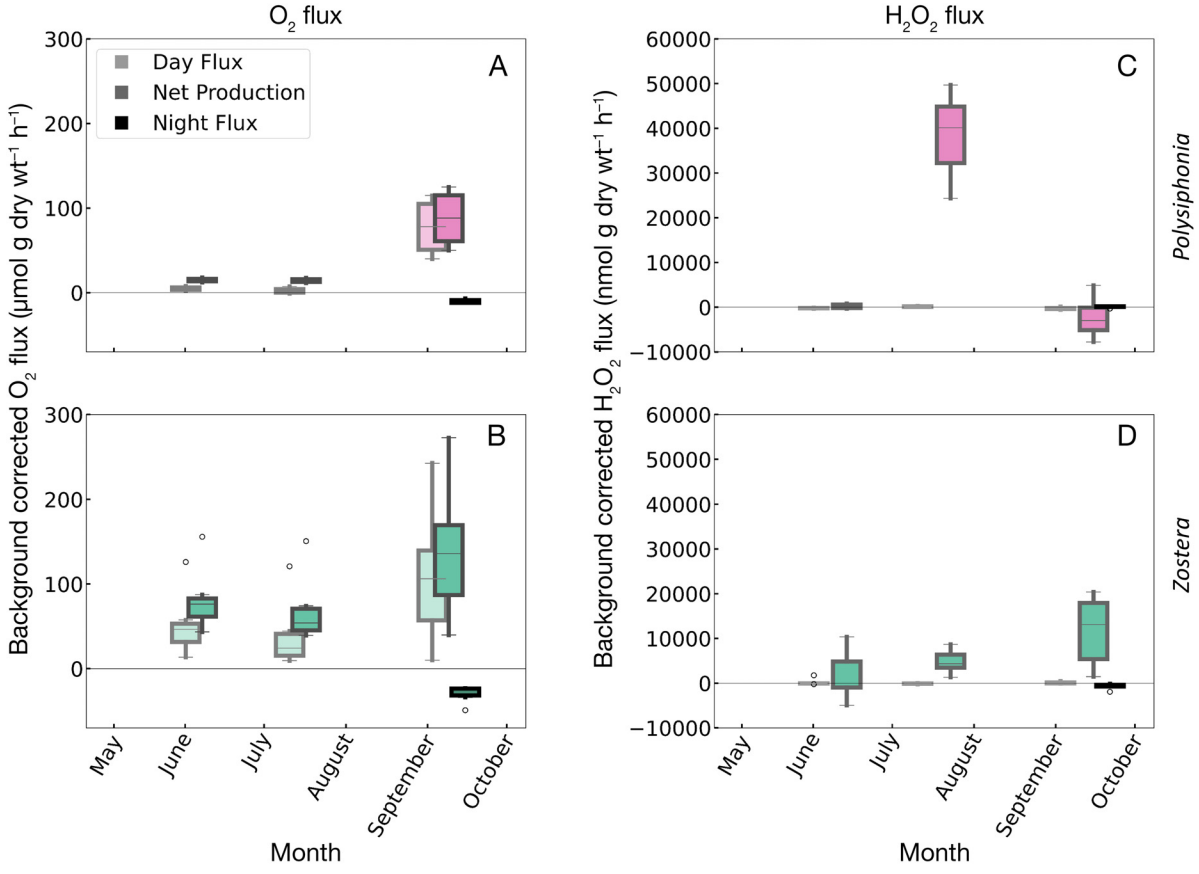

Fig. 3. Biomass-normalized, seawater-corrected (A,B) O_2 and (C,D) H_2O_2 flux within (A,C) *Polysiphonia* and (B,D) *Zostera* incubations across all 3 sample periods (June, July, and September). Boxplots: from biological replicates, with the middle 50th percentile (box), median (horizontal line), middle 90th percentile (vertical lines), and outliers (open circles). Day fluxes (gray outline, light pink or green fill) and net production (dark gray outline, dark pink, dark green fill) shown for June, July, and September. Night fluxes (black outline) were only measured in September. See Table S2 for data

Hydrogen peroxide flux and net production (see Eqs. 4 & 5) in *Zostera* and *Polysiphonia* incubations were both positive and negative (all seawater-corrected and biomass-normalized, see Table S2 for hydrogen peroxide data), indicating that the addition of photosynthetic macrophytes had a nonuniform impact on hydrogen peroxide dynamics, contributing to consumption and production across the sampling period. Specifically, hydrogen peroxide fluxes from *Polysiphonia* ranged from −271.7 ± 269.0 nmol g dry wt^{-1} h^{-1} (September) to 132.2 ± 101.1 nmol g dry wt^{-1} h^{-1} (July), with significant monthly differences only between June and July (ANOVA p = 0.010 for June and July, yet 0.079 for comparing all months, Fig. 3C). In contrast, hydrogen peroxide fluxes from *Zostera* were highest in June (149.9 ± 612.2 nmol g dry wt^{-1} h^{-1}) and lowest in July (−115.0 ± 77.8 nmol g dry wt^{-1} h^{-1}, Fig. 3D), with only a statistically significant difference in fluxes between July and September (ANOVA p = 0.014, Table S3). Evening hydrogen peroxide fluxes (September only) were positive (62.8 ± 214.7 nmol g dry wt^{-1} h^{-1}) from *Polysiphonia*, reflecting increased production, whereas for *Zostera* they were negative (−722.9 ± 576.8 nmol g dry wt^{-1} h^{-1}), reflecting greater consumption by the seagrass (Fig. 3C,D). Across all months, $NP_{H_2O_2}$ by *Polysiphonia* mirrored the fluxes with lowest net production in September (−2212 ± 4615 nmol g dry wt^{-1} h^{-1}) and the highest in July (38 030 ± 10 450 nmol g dry wt^{-1} h^{-1}) (Fig. 3C). Alternatively, the $NP_{H_2O_2}$ within *Zostera* incubations did not span as large of a range and were lowest in June (1496 ± 4619 nmol g dry wt^{-1} h^{-1}) and highest in September (19 103 ± 22 660 nmol g dry wt^{-1} h^{-1}) (Fig. 3D). Areal net hydrogen peroxide production by *Polysiphonia* was essentially zero for June and September (0.1 ± 0.1 mmol m^{-2} d^{-1} and 0.0 ± 0.1 mmol m^{-2} d^{-1}, respectively), yet higher in July (9.8 ± 2.7 mmol m^{-2} d^{-1}) (Fig. 4D). The areal net hydrogen production rates by *Zostera* were similar in magnitude to those of *Polysiphonia* and increased

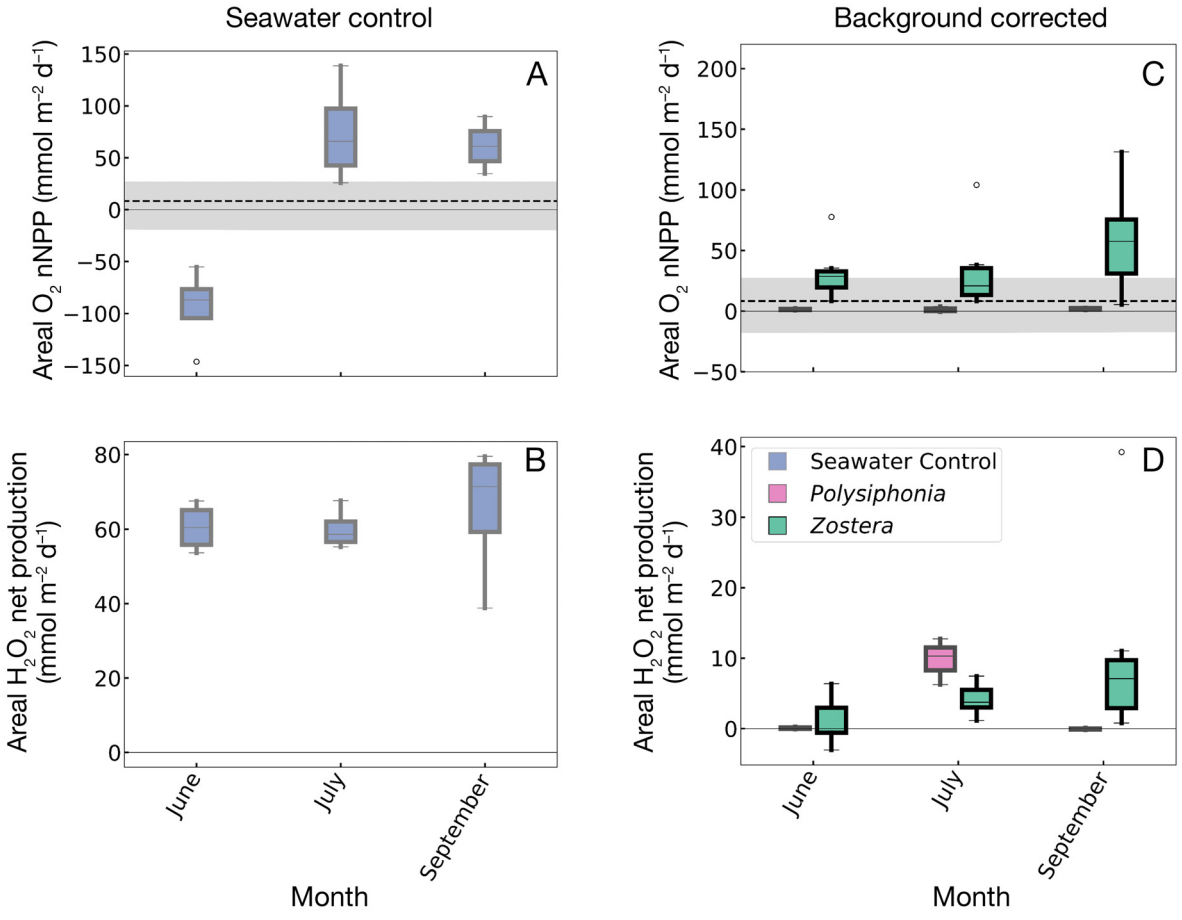

Fig. 4. (A,B) Seawater control data were used to (C,D) background seawater correct *Polysiphonia* and *Zostera* data for (A,C) areal net primary production (NPP, O_2) and (B,D) areal net H_2O_2 production for each sample period integrated over a depth of 2 m. Horizontal dashed line for O_2 fluxes: average net ecosystem metabolism (NEM) gathered from previous data; gray shading: SD of these previous data (8 ± 54 mmol m^{-2} d^{-1}; Duarte et al. 2010, Long et al. 2015, Long et al. 2019). See Table S2 for data

throughout the summer, starting at 0.9 ± 2.8 mmol m^{-2} d^{-1} (June) and rising to 10.3 ± 12.3 mmol m^{-2} d^{-1} (September) (Fig. 4D).

3.2.3. Hydrogen peroxide decay rate constants

Changes in the abundance of $^{34}O_2$ from Analysis 1 (reflecting the combination of naturally occurring ^{16}O-^{18}O plus the emergence of ^{17}O-^{17}O deriving from H_2O_2 oxidation in the dissolved O_2 pool and corrected for photosynthetic activity) generally increased slightly from the initial natural baseline composition over time. In contrast, for the abundance of $^{34}O_2$ from Analysis 2 (reflecting the summed changes in ^{16}O-^{18}O, the ^{17}O-^{17}O produced from H_2O_2 oxidation as well as the ^{17}O-^{17}O in the remaining H_2O_2 pool, and corrected for photosynthetic activity), the change in $^{34}O_2$ content decreased sharply for all incubations, reflecting loss of $H_2{}^{17}O_2$ by reduction to H_2O through peroxidase-like pathways — which is calculated based on the difference between the starting $H_2{}^{17}O_2$ composition and Analysis 2 (Fig. S3).

Based on the isotopic tracking of the fate of H_2O_2 in the decay incubations, hydrogen peroxide pseudo first-order decay rate constants ($k_{loss,isotope}$) were lowest in the seawater control and fastest for *Polysiphonia* incubations during all months (Table 1). In all incubations, the hydrogen peroxide in *Polysiphonia* and *Zostera* decayed within the first 0.3 h (July) to 4.2 h (June) and those in the seawater control decayed within 3.9 h (September) to 4.4 h (June and July). Values of $k_{loss,isotope}$ in the seawater control ranged from 0.314 h^{-1} (June) to 0.706 h^{-1} (July). Comparatively, $k_{loss,isotope}$ ranged from 0.729 h^{-1} (June) to 9.090 h^{-1} (July) for *Polysiphonia* and from 0.371 h^{-1} (June) to 0.897 h^{-1} (September) for *Zostera*. Averaging the decay rate constants of all species, June exhibited the lowest

Table 1. Decay rates of H_2O_2, calculated from the isotope spike addition experiments. $k_{loss,isotope} = k_{ox} + k_{red}$, where k_{ox} is the decay rate constant from the oxidative pathway and k_{red} is the decay rate constant from the reductive pathway. k_{ox}:k_{red} is the ratio between the 2 decay rates, where k_{ox}:$k_{red} < 1$ represents a net reductive pathway. $k_{loss,POHPPA}$, the decay rate constant measured using the POHPPA (4-hydroxyphenylacetic acid) method, is also displayed for reference. Top half of the table: individual rates across each species and sample period. Bottom half of the table: the averages ± SD per species and per sample period, respectively

Species	Month	$k_{loss,isotope}$ (h^{-1})	k_{ox} (h^{-1})	k_{red} (h^{-1})	k_{ox}:k_{red}	$k_{loss,POHPPA}$ (h^{-1})
Individual rates						
Water	June	0.314	0.058	0.255	0.229	–
Polysiphonia	June	0.729	0.000	0.733	0.000	–
Zostera	June	0.371	0.056	0.315	0.178	–
Water	July	0.706	0.046	0.660	0.057	0.140
Polysiphonia	July	9.09	0.013	9.08	0.001	0.72
Zostera	July	1.09	0.000	1.09	0.000	0.43
Water	September	0.317	0.061	0.257	0.236	0.205
Polysiphonia	September	1.05	0.079	0.973	0.081	0.67
Zostera	September	0.897	0.037	0.860	0.043	0.384
Averages ± SD						
Water		0.446 ± 0.184	0.055 ± 0.006	0.391 ± 0.190	0.174 ± 0.083	0.173 ± 0.033
Polysiphonia		3.62 ± 3.87	0.030 ± 0.034	3.59 ± 3.88	0.027 ± 0.038	0.696 ± 0.027
Zostera		0.784 ± 0.303	0.031 ± 0.023	0.756 ± 0.326	0.074 ± 0.076	0.406 ± 0.022
June		0.471 ± 0.184	0.038 ± 0.027	0.434 ± 0.213	0.136 ± 0.098	–
July		3.63 ± 3.87	0.020 ± 0.019	3.61 ± 3.87	0.020 ± 0.027	0.430 ± 0.238
September		0.755 ± 0.316	0.059 ± 0.017	0.697 ± 0.314	0.120 ± 0.083	0.419 ± 0.212

average decay rate constant (0.446 ± 0.184 h^{-1}) and July the highest (3.63 ± 3.87 h^{-1}). Given that these rate constants were measured using a 500 nM addition, these decay rate constants could be an overestimate relative to those from the environment with lower concentrations, assuming no change in this decay constant and that the reaction exhibits first-order decay.

For all species, values of k_{ox} were lower than k_{red} (k_{ox}:$k_{red} < 1$), indicating the dominance of reductive hydrogen peroxide loss across all months (Table 1). Compared to other incubations, the seawater control showed the highest ratio of k_{ox}:k_{red} for each month, with an average of 0.174 ± 0.083 across all sampling events, ranging from 0.057 (July) to 0.236 (September). *Polysiphonia* and *Zostera* were much lower, with average k_{ox}:k_{red} ratios of 0.027 ± 0.038 and 0.074 ± 0.076, respectively, ranging from 0.000 (June) to 0.081 (September) and 0.000 (July) to 0.178 (June), respectively. Averaging all species together, July was the most reductive month (k_{ox}:k_{red} = 0.020 ± 0.027) and June was the least (k_{ox}:k_{red} = 0.136 ± 0.098). Comparatively, the hydrogen peroxide pseudo first-order decay rate constants measured using the POHPPA method ($k_{loss,POHPPA}$) showed the same trends across species and months as those measured using the isotope method ($k_{loss,isotope}$), yet the decay rate constants derived from the POHPPA method were consistently lower (see Text S3).

4. DISCUSSION

4.1. Rapid oxygen production leads to net autotrophy

This study characterizes the individual contribution of primary producers to the oxygen flux within a seagrass ecosystem, demonstrating that *Zostera* contributed substantially to oxygen NPP, while *Polysiphonia* produced comparatively less. As expected, incubations with *Polysiphonia* and *Zostera* exhibited net photosynthesis during the day that exceeded the daily rates of respiration, suggesting that the observed components were likely contributing to net autotrophy. These observed oxygen trends agree with previous studies that measured oxygen rates within seagrass ecosystems (Duarte et al. 2010, Long et al. 2019).

While $NP_{H_2O_2}$ was also elevated during the daytime (see below for further discussion), hydrogen peroxide fluxes did not appear to be directly linked to major metabolic oxygen cycling (i.e. photosynthesis and respiration). When comparing fluxes and net production of hydrogen peroxide and oxygen across all species and sampling events, there were few instances with significant correlation ($R^2 > 0.63$ and *t*-test $p < 0.05$, Table S4). The few instances exhibiting significant correlations included comparison of fluxes in

incubations of *Polysiphonia* in September (R^2 = 0.761 and *t*-test p = 0.017), the net production values for *Polysiphonia* in July (R^2 = 0.828 and *t*-test p = 0.037), and net production values for *Zostera* for July and September (R^2 = 0.670 and 0.701 and *t*-test p = 0.019 and 0.007, respectively; Table S4). Metabolic processes of seagrasses are complex and poorly understood (Larkum et al. 2006), yet this lack of consistent correlation suggests that hydrogen peroxide production is predominantly controlled by processes other than those that may directly link oxygen and hydrogen peroxide (e.g. photosynthesis and respiration) or that the timescales of these 2 fluxes vary so much that links between environmental observations would not be predicted. Below, we discuss the hydrogen peroxide production and decay dynamics observed within this study, noting where additional research is required to further understand the hydrogen peroxide cycling dynamics within seagrass ecosystems. For additional discussion on the oxygen dynamics observed within this study, see Text S2.

4.2. Elevated hydrogen peroxide steady-state concentrations and decay in seagrass ecosystems

The steady-state hydrogen peroxide concentrations found in this study are similar to hydrogen peroxide concentrations in other coastal environments, such as coral reefs and estuaries (Price et al. 1994, Shaked & Armoza-Zvuloni 2013, Hopwood et al. 2017). Seawater control steady-state hydrogen peroxide concentrations (i.e. the concentration at the beginning of the incubations) ranged between 60.3 ± 34.3 (July) and 369.7 ± 71.6 nM (September) (Fig. 2B). Despite differences in the incubation approached used, hydrogen peroxide concentrations measured here are similar to other coastal environments, such as those observed within surface waters in the Mediterranean (24–143 nM), around coral reefs in the Red Sea (~77–88 nM), and within the Chesapeake Bay (~440 nM) (Price et al. 1994, O'Sullivan et al. 2005, Shaked & Armoza-Zvuloni 2013, Hopwood et al. 2017). The similarity across measurement approaches provides reassurance that artifacts from bottle effects were likely minimal.

Steady-state concentrations are a combination of production and decay, and our study documented high hydrogen peroxide decay rate constants (Table 1) that are comparable to previous observations in other coastal and open ocean environments. Across all months, on average, hydrogen peroxide decay rate constants within seawater (0.446 ± 0.184 h^{-1}, Table 1) are an order of magnitude or more higher than those observed in the open ocean (0.0247 ± 0.0024 to 0.0281 ± 0.0019 h^{-1}; Sutherland et al. 2021), reef waters (average 0.014 ± 0.011 h^{-1}; Shaked & Armoza-Zvuloni 2013), and as dark decay rates in the Atlantic Ocean (0.0044 ± 0.0008 to 0.0113 ± 0.0025 h^{-1}; Yuan & Shiller 2001). The addition of *Polysiphonia* and *Zostera* further accelerated the decay of hydrogen peroxide within this study, with decay rate constants averaging 3.62 ± 3.87 and 0.784 ± 0.303 h^{-1}, respectively (Table 1). All such decay rate constants, however, pale in comparison to rates documented in waters collected at the surface of corals (averaged 18 ± 14 h^{-1}; Shaked & Armoza-Zvuloni 2013). The relatively high decay rate constants here compared to other ecosystems could be due to microbial processes, enzymatic activity (i.e. catalases and/or peroxidases), and/or other abiotic factors such as high content of dissolved metals and/or organic matter (i.e. DOC or CDOM) (Moffett & Zika 1987, Moffett & Zafiriou 1993, Hansel 2017). In fact, as a coastal ecosystem with inputs from land, it is not surprising that seagrass ecosystems would exhibit elevated concentrations of dissolved metals, DOC, and/or CDOM (Stabenau et al. 2004).

4.3. Potential hydrogen peroxide production mechanisms

While this study did not specifically determine the mechanism(s) of hydrogen peroxide production, the high fluxes of hydrogen peroxide associated with photosynthetic macrophytes point to potential production pathways. Hydrogen peroxide can be produced directly or through a superoxide intermediate. Unlike superoxide, hydrogen peroxide can pass across biological membranes and thus potential sources may include both intracellular and extracellular processes (Korshunov & Imlay 2002, Diaz et al. 2013, Armoza-Zvuloni & Shaked 2014). In seawater, hydrogen peroxide may be produced from superoxide via reaction with a combination of different components including microbial activity, dissolved metals, CDOM, and/or other small organic molecules (Moffett & Zika 1987, Anderson et al. 2016). In our study, the inclusion of *Polysiphonia* and *Zostera* significantly enhanced rates of hydrogen peroxide production during specific months compared to the seawater control incubations, with most of the variation occurring during June for *Polysiphonia* (*t*-test p = 0.009; Table S3) and July for *Zostera* (*t*-test p = 0.004, Table S3). Although to our knowledge, hydrogen per-

oxide production mechanisms by these specific species have not been previously studied, macroalgae are generally known to produce hydrogen peroxide (see Hansel & Diaz 2021 and references within). In macroalgae, intracellular hydrogen peroxide production is generated as a byproduct of cellular processes along the electron transport chain in mitochondria or chloroplasts or via enzymes and organelles (e.g. peroxisomes) (Sewelam et al. 2014). In the absence of stress, extracellular hydrogen peroxide production can be a consequence of physiological processes regulated by respiratory burst oxidase homologs (*Rboh*, including NOX homologs), oligosaccharide oxidases, and/or amino oxidases (Collén & Pedersén 1996, Hou et al. 2015, McDowell et al. 2015). Intracellular and extracellular production can also increase in the presence of stress (i.e. heat stress, osmotic stress, wounding, pathogen infection, and grazers) (Ross & Alstyne 2007, Wang et al. 2018). Given that peroxisomes and *Rboh* genes are identified within the *Z. marina* genome (Olsen et al. 2016), it is possible that *Z. marina* produces and regulates hydrogen peroxide through similar mechanisms as macroalgae. In this study, large variations were observed in hydrogen peroxide fluxes amongst individuals (i.e. high SDs, Fig. 3C,D, Table S2), which is understandable if hydrogen peroxide is produced by such processes that are controlled by environmental and physiological processes that may differ over time and amongst individual organisms. Additionally, given that this study incubated the macrophytes within closed systems, there could be additional processes that alter the hydrogen peroxide fluxes that are not accounted for in this study, such as variable water flow, changes in diffusive boundary conditions, physical disturbances, and/or alterations in the environmental biogeochemical conditions.

Due to the general increase in macrophyte-based hydrogen peroxide production during the daytime, it is possible that daytime processes other than those directly linked to oxygen production (see Section 4.1) could contribute to the production of hydrogen peroxide. These might include increased production by metabolic or co-metabolic processes, enzymes (i.e. as NAD(P)H oxidoreductase enzymes, heme peroxidases, and/or glutathione reductases) (Diaz et al. 2013, 2019, Andeer et al. 2015), and/or exudates (i.e. reactive metabolites) (Kieber et al. 2003, Wuttig et al. 2013). For example, light-dependent production of photosynthetic NADPH as a substrate for NOX and/or passive diffusion of hydrogen peroxide produced during the light reactions of photosynthesis could lead to increased hydrogen peroxide production with elevated light (Collén & Pedersén 1996, McDowell et al. 2015). Indeed, multiple processes likely contribute to complex variations in peroxide dynamics over space and time in both the macroalgae and seagrass as well as possibly their associated epiphytes.

4.4. The fate of hydrogen peroxide

Hydrogen peroxide exhibited rapid decay, reflecting high rates of turnover in the seagrass meadow studied here. Based on k_{loss}, the half-life of hydrogen peroxide in the seawater control (average 2.0 ± 0.5 h) was noticeably longer than those observed in the presence of *Polysiphonia* and *Zostera* (average 0.6 ± 0.4 and 1.1 ± 0.7 h, respectively). These half-lives are similar to those previously observed in a lagoon near a coral reef (0.5 to 4 h), yet significantly shorter than those analyzed in Florida coastal waters (10 h) and in oligotrophic waters off the coast of Florida (120 h) (Petasne & Zika 1997) as well as in the Gulf of Aqaba (16 to 18 h) (Shaked & Armoza-Zvuloni 2013). While previous studies have not calculated areal net production rates of hydrogen peroxide, our results suggest that seawater contributed to relatively consistent hydrogen peroxide production across the seasons at a rate ranging from ~60 to 65 mmol d^{-1} m^{-2}, and that *Polysiphonia* and *Zostera* further accelerated areal net production by up to 10 mmol d^{-1} m^{-2} for both species. The rapid production and decay of hydrogen peroxide by *Polysiphonia* and *Zostera* suggests that the hydrogen peroxide is unlikely to be transported more than several hundred meters (e.g. ~100 to 350 m transport with 0.05 m s^{-1} tidal currents) beyond the boundaries of the seagrass meadow depending on various environmental factors (i.e. mixing dynamics, bathymetry, species composition, etc.). However, given that these hydrogen peroxide areal net production rates are on the same order of magnitude as the oxygen areal net production rates, this suggests that hydrogen peroxide may be an important redox-active reactant within the seagrass ecosystem or immediately adjacent environments. Further exploration of the spatial and temporal distribution of hydrogen peroxide throughout and adjacent to seagrass ecosystems is needed to test this hypothesis.

Our results also indicate that hydrogen peroxide was lost predominantly through reductive, peroxidase-like decay pathways. This finding contrasts with previous studies in the open ocean, which observed hydrogen peroxide acting primarily as a reductant (or being oxidized) that was lost mainly through catalase-

like pathways, leading to enhanced recycling of molecular oxygen (Sutherland et al. 2021). Similarly, another previous study in Martha's Vineyard Sound (~5 km away from our study location) attributed 65–80% of hydrogen peroxide decay to catalase-like activity (which leads to equal parts oxidative and reductive loss) (Moffett & Zafiriou 1990). While many studies have documented both catalase and peroxidase activity within seagrasses and macroalgae (Dummermuth et al. 2003, Weinberg et al. 2013, Liu et al. 2016, Zang et al. 2018, Satoh et al. 2019, Pei et al. 2024), the present study is the first to quantify the percentage of hydrogen peroxide that is decaying through different pathways within seagrass ecosystems. All incubations exhibited more reductive than oxidative H_2O_2 loss, suggesting that hydrogen peroxide was mainly lost through peroxidase-like decay pathways (Fig. 5). In fact, an average of 62 to 90% of the hydrogen peroxide produced decayed through peroxidase-like pathways, thus reducing 81 to 95% of produced hydrogen peroxide to water. The presence of *Polysiphonia* and *Zostera* resulted in even higher percentages of hydrogen peroxide lost through the peroxidase-like pathways (70 to 100%) leading to the return of the majority of H_2O_2 to water (85 to 100%).

The reduction of hydrogen peroxide may occur through a range of pathways, including direct reactions with peroxidase-like enzymes and/or reduced chemical species within the environment. In the case of the latter, hydrogen peroxide can serve as an oxidant of carbon and various dissolved metals (i.e. Fe(II) and Mn(II)) to form metal oxides in some cases. Reaction between hydrogen peroxide and Fe(II) leads to the formation of the hydroxyl radical (known as the Fenton reaction), a strong and indiscriminant redox reactant (Klinkhammer et al. 1982, Illés et al. 2019). Direct decay via peroxidases is also probable, given the diversity of roles peroxidases play in seaweeds, such as wound repair, cell-signaling, and defense (Ross et al. 2005, Cosse et al. 2009, Punitha et al. 2018). Although the driving force behind the rapid reductive decay of hydrogen peroxide in this system remains unresolved, it is important to investigate further because these reactions can have large implications on metal bioavailability (via speciation) and carbon remineralization (via hydroxyl radical formation) (Winterbourn 1995, Illés et al. 2019, Jones et al. 2020).

4.5. Larger implications

As seagrass ecosystems are impacted by many stressors, largely anthropogenic in origin (Short et al. 2011, Waycott et al. 2019), it is vital to understand how the dominant macrophytes of the system will respond individually and contribute to the overall biogeochemistry of the environment, especially given future predicted changes in ecosystem composition and environmental conditions (Chefaoui et al. 2021). Here we characterized and quantified the specific roles that both *Polysiphonia* and *Zostera* play as dominant macrophytes in both oxygen and hydrogen peroxide budgets. These potential impacts on the biogeochemical cycles varied temporally and across individuals for both *Polysiphonia* and *Zostera*, suggesting that the ecosystem processes are influenced by a confluence of both environmental variables and organismal physiology. With a changing climate, additional studies that investigate organismal response to increased stress (i.e. heat, light, and osmotic stress) in relation to hydrogen peroxide production are crucial, since accelerated metabolisms could increase the release of intracellular hydrogen peroxide and other substrates that lead to ROS production or consumption (i.e. NADPH and other enzymes and exudates) (Armoza-Zvuloni & Shaked 2014, Diaz & Plummer 2018, Diaz et al. 2019). Specifically, while the production and decay mechanisms of ROS remain unclear, this study shows that hydrogen peroxide is being produced on a spatial scale at the same order of magnitude as oxygen, suggesting that ROS dynamics within seagrass ecosystems are central to the biogeochemical landscape.

As ROS can play critical roles in modulating the redox state of the ecosystem, environmental pressures that alter ROS cycling and production can have further cascading effects on other biogeochemical cycles, such as oxygen, carbon, and trace metals (Moffett & Zika 1987, Sutherland et al. 2021). In the first known study to investigate and quantify the fate of hydrogen peroxide within a seagrass meadow, we found that hydrogen peroxide was lost mainly through the peroxidase-like pathway (62 to 100%). This equates to a 70 to 100% reduction of hydrogen peroxide to water. Thus hydrogen peroxide is acting as an oxidant, which has not been previously considered alongside most seagrass ecosystems dynamics that rely on biogeochemical cycling within seagrasses, such as oxygen production, carbon fluxes, and sequestration potential within seagrass beds (Enríquez et al. 1993, Berger et al. 2020). Looking forward, characterizing the role of ROS in biogeochemical cycling may be relevant for accurately assessing the importance of seagrass ecosystems to coastal environments and communities.

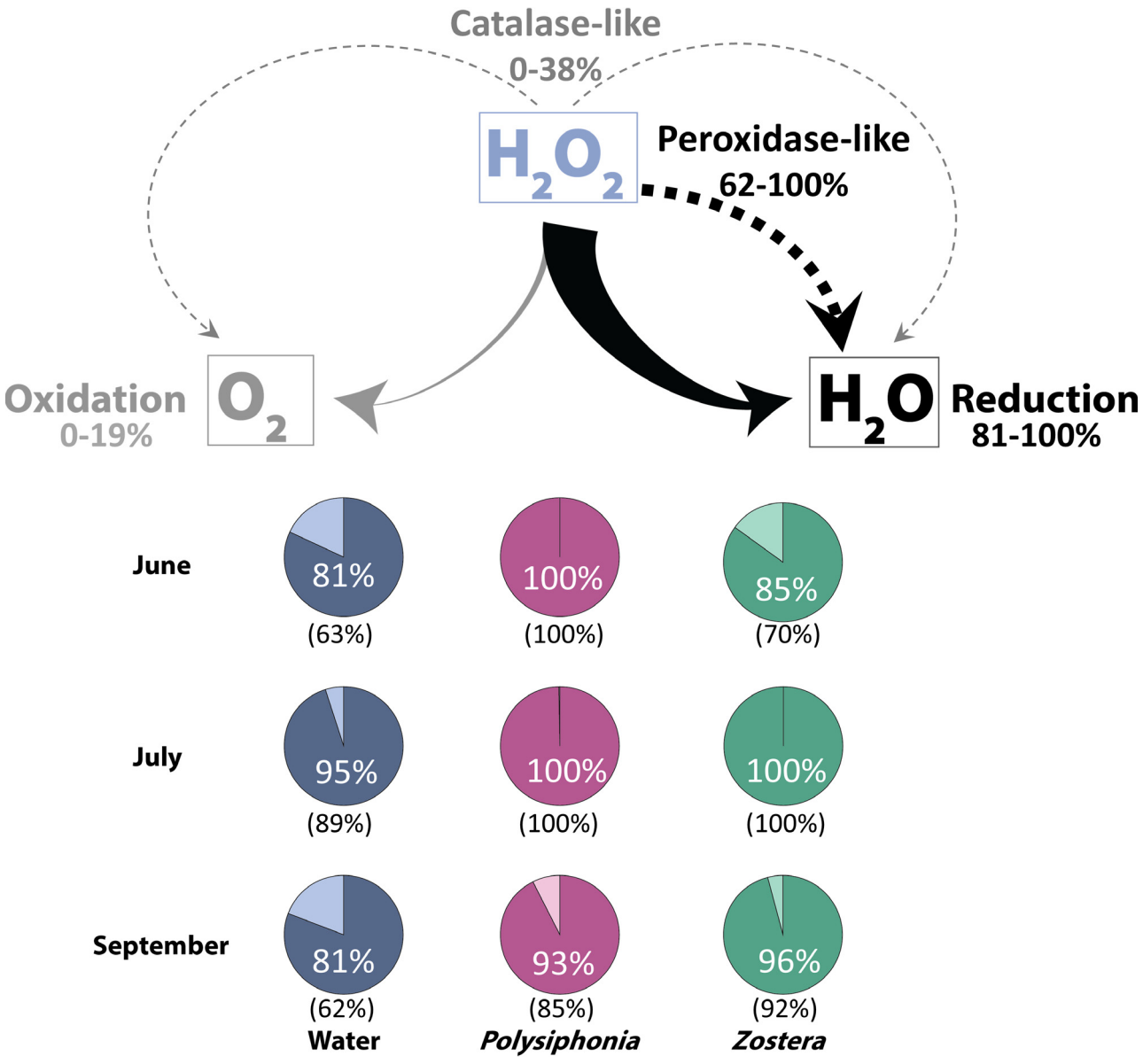

Fig. 5. The different decay pathways (top) for H_2O_2 decay, either through oxidation to O_2 or reduction to H_2O, and the peroxidase-like and catalase-like pathways; the arrow thickness is proportional to the decay pathway, with the percentage indicating the range across all incubations. Pie charts show the specific proportions of oxidation (light shades) and reduction (dark shades) for water, *Polysiphonia*, and *Zostera* during each sample period. Percentages stated within the pie charts refer to the reductive pathway, and percentages stated below the pie charts in parentheses refer to the peroxidase-like pathway

Data availability. Data is available online at seanoe.org: Grabb KC, Wankel SD, Sutherland KM, Bowman SH, Long MH, Hansel CM (2024) Data investigating hydrogen peroxide fluxes and fate in a temperate seagrass ecosystem. SEANOE, https://doi.org/10.17882/100247

Acknowledgements. This work was funded by grants from Schmidt Marine Technology Partners (G-2010-59878 to C.M.H.), NSF GRFP (2016230168 to K.C.G.), WHOI Ocean Ventures Fund (2021 to K.C.G.), Agouron Institute Geobiology Fellowship (K.M.S.), and MIT (Wellington and Irene Loh Fund to K.C.G.). We acknowledge and thank the many helpers who lent a hand collecting fieldwork data, including Dr. Bayleigh Benner, Solomon Chen, Sophie Ferguson, Erica Herrera, Mallory Kastner, Dr. Chadlin Ostrander, Rachel Phillips, Lina Taenzer, Luciana Villarroel, and Dr. Yi Wang.

LITERATURE CITED

Achamlale S, Rezzonico B, Grignon-Dubois M (2009) Evaluation of *Zostera* detritus as a potential new source of zosteric acid. J Appl Phycol 21:347–352

Andeer PF, Learman DR, McIlvin M, Dunn JA, Hansel CM (2015) Extracellular haem peroxidases mediate Mn(II) oxidation in a marine *Roseobacter* bacterium via superoxide production: peroxidases mediate superoxide-based Mn oxidation. Environ Microbiol 17:3925–3936

Anderson A, Laohavisit A, Blaby IK, Bombelli P and others (2016) Exploiting algal NADPH oxidase for biophotovoltaic energy. Plant Biotechnol J 14:22–28

Armoza-Zvuloni R, Shaked Y (2014) Release of hydrogen peroxide and antioxidants by the coral *Stylophora pistillata* to its external milieu. Biogeosciences 11:4587–4598

Badger MR, von Caemmerer S, Ruuska S, Nakano H (2000) Electron flow to oxygen in higher plants and algae: rates and control of direct photoreduction (Mehler reaction) and rubisco oxygenase. Philos Trans R Soc B 355: 1433–1446

Berger AC, Berg P, McGlathery KJ, Delgard ML (2020) Long-term trends and resilience of seagrass metabolism: a decadal aquatic eddy covariance study. Limnol Oceanogr 65:1423–1438

Bond RJ, Hansel CM, Voelker BM (2020) Heterotrophic bacteria exhibit a wide range of rates of extracellular production and decay of hydrogen peroxide. Front Mar Sci 7:72

Brodersen KE, Kühl M (2023) Photosynthetic capacity in seagrass seeds and early-stage seedlings of *Zostera marina*. New Phytol 239:1300–1314

Celebi-Ergin B, Zimmerman RC, Hill VJ (2022) Photorespiration in eelgrass (*Zostera marina* L.): a photoprotection mechanism for survival in a CO_2-limited world. Front Plant Sci 13:1025416

Chefaoui RM, Duarte CM, Tavares AI, Frade DG, Cheikh MAS, Ba AM, Serrao EA (2021) Predicted regime shift in the seagrass ecosystem of the Gulf of Arguin driven by climate change. Glob Ecol Conserv 32:e01890

Cho SH, Heo SJ, Yang HW, Ko EY and others (2019) Protective effect of 3-bromo-4,5-dihydroxybenzaldehyde from *Polysiphonia morrowii* Harvey against hydrogen peroxide-induced oxidative stress *in vitro* and *in vivo*. J Microbiol Biotechnol 29:1193–1203

Collén J, Pedersén M (1996) Production, scavenging and toxicity of hydrogen peroxide in the green seaweed *Ulva rigida*. Eur J Phycol 31:265–271

Coogan J, Long MH (2023) Development and deployment of a long-term aquatic eddy covariance system. Limnol Oceanogr Methods 21:552–562

Cooper WJ, Zepp RG (1990) Hydrogen peroxide decay in waters with suspended soils: evidence for biologically mediated processes. Can J Fish Aquat Sci 47:888–893

Cosse A, Potin P, Leblanc C (2009) Patterns of gene expression induced by oligoguluronates reveal conserved and environment-specific molecular defense responses in the brown alga *Laminaria digitata*. New Phytol 182:239–250

Diaz JM, Plummer S (2018) Production of extracellular reactive oxygen species by phytoplankton: past and future directions. J Plankton Res 40:655–666

Diaz JM, Hansel CM, Voelker BM, Mendes CM, Andeer PF, Zhang T (2013) Widespread production of extracellular superoxide by heterotrophic bacteria. Science 340: 1223–1226

Diaz JM, Plummer S, Hansel CM, Andeer PF, Saito MA, McIlvin MR (2019) NADPH-dependent extracellular superoxide production is vital to photophysiology in the marine diatom *Thalassiosira oceanica*. Proc Natl Acad Sci USA 116:16448–16453

Do SH, Batchelor B, Lee HK, Kong SH (2009) Hydrogen peroxide decomposition on manganese oxide (pyrolusite): kinetics, intermediates, and mechanism. Chemosphere 75:8–12

Dole M, Rudd DP, Muchow GR, Comte C (1952) Isotopic composition of oxygen in the catalytic decomposition of hydrogen peroxide. J Chem Phys 20:961–968

Duarte CM, Chiscano CL (1999) Seagrass biomass and production: a reassessment. Aquat Bot 65:159–174

Duarte CM, Marbà N, Gacia E, Fourqurean JW, Beggins J, Barrón C, Apostolaki ET (2010) Seagrass community metabolism: assessing the carbon sink capacity of seagrass meadows. Glob Biogeochem Cycles 24:GB4032

Dummermuth AL, Karsten U, Fisch KM, König GM, Wiencke C (2003) Responses of marine macroalgae to hydrogen-peroxide stress. J Exp Mar Biol Ecol 289:103–121

Eisenhut M, Ruth W, Haimovich M, Bauwe H, Kaplan A, Hagemann M (2008) The photorespiratory glycolate metabolism is essential for cyanobacteria and might have been conveyed endosymbiontically to plants. Proc Natl Acad Sci USA 105:17199–17204

Enríquez S, Duarte CM, Sand-Jensen K (1993) Patterns in decomposition rates among photosynthetic organisms: the importance of detritus C:N:P content. Oecologia 94: 457–471

Fridovich I (1998) Oxygen toxicity: a radical explanation. J Exp Biol 201:1203–1209

Grabb KC, Kapit J, Wankel SD, Manganini K, Apprill A, Armenteros M, Hansel CM (2019) Development of a handheld submersible chemiluminescent sensor: quantification of superoxide at coral surfaces. Environ Sci Technol 53:13850–13858

Greco M, Sáez CA, Contreras RA, Rodríguez-Rojas F, Bitonti MB, Brown MT (2019) Cadmium and/or copper excess induce interdependent metal accumulation, DNA methylation, induction of metal chelators and antioxidant defences in the seagrass *Zostera marina*. Chemosphere 224:111–119

Hansel CM (2017) Manganese in marine microbiology. Adv Microb Physiol 70:37–83

Hansel CM, Diaz JM (2021) Production of extracellular reactive oxygen species by marine biota. Annu Rev Mar Sci 13:177–200

Heller MI, Croot PL (2010) Kinetics of superoxide reactions with dissolved organic matter in tropical Atlantic surface waters near Cape Verde (TENATSO). J Geophys Res Oceans 115:C12038

Hopwood MJ, Rapp I, Schlosser C, Achterberg EP (2017) Hydrogen peroxide in deep waters from the Mediterranean Sea, South Atlantic and South Pacific Oceans. Sci Rep 7:43436

Hou Y, Wang J, Simerly T, Jin W, Zhang H, Zhang Q (2015) Hydrogen peroxide released from *Pyropia yezoensis* induced by oligo-porphyrans: mechanisms and effect. J Appl Phycol 27:1639–1649

Illés E, Mizrahi A, Marks V, Meyerstein D (2019) Carbonate-radical-anions, and not hydroxyl radicals, are the products of the Fenton reaction in neutral solutions containing bicarbonate. Free Radic Biol Med 131:1–6

Jensen S, Kühl M, Glud R, Jørgensen L, Priemé A (2005) Oxic microzones and radial oxygen loss from roots of *Zostera marina*. Mar Ecol Prog Ser 293:49–58

Jones MR, Luther GW, Tebo BM (2020) Distribution and concentration of soluble manganese(II), soluble reactive Mn(III)-L, and particulate MnO_2 in the Northwest Atlantic Ocean. Mar Chem 226:103858

Jordà G, Marbà N, Duarte CM (2012) Mediterranean seagrass vulnerable to regional climate warming. Nat Clim Change 2:821–824

Kieber DJ, Blough NV (1990) Determination of carbon-centered radicals in aqueous solution by liquid chromatography with fluorescence detection. Anal Chem 62: 2275–2283

Kieber DJ, Peake BM, Scully NM (2003) Reactive oxygen species in aquatic ecosystems. In: Helbling EW, Zagarese H (eds) UV effects in aquatic organisms and ecosystems. Royal Society of Chemistry, Cambridge, p 251–288

Klinkhammer G, Heggie DT, Graham DW (1982) Metal diagenesis in oxic marine sediments. Earth Planet Sci Lett 61:211–219

Koppenol WH (1993) The centennial of the Fenton reaction. Free Radic Biol Med 15:645–651

Korshunov SS, Imlay JA (2002) A potential role for periplasmic superoxide dismutase in blocking the penetration of external superoxide into the cytosol of Gram-negative bacteria. Mol Microbiol 43:95–106

Kuwae T, Hori M (eds) (2019) Blue carbon in shallow coastal ecosystems: carbon dynamics, policy, and implementation. Springer, Singapore

Larkum AWD, Orth RJ, Duarte CM (eds) (2006) Seagrasses: biology, ecology, and conservation. Springer, Dordrecht

Lester Y, Sharpless CM, Mamane H, Linden KG (2013) Production of photo-oxidants by dissolved organic matter during UV water treatment. Environ Sci Technol 47: 11726–11733

Lin H, Sun T, Zhou Y, Zhang X (2016) Anti-oxidative feedback and biomarkers in the intertidal seagrass *Zostera japonica* induced by exposure to copper, lead and cadmium. Mar Pollut Bull 109:325–333

Liu J, Tang X, Wang Y, Zang Y, Zhou B (2016) A *Zostera marina* manganese superoxide dismutase gene involved in the responses to temperature stress. Gene 575: 718–724

Long MH, Berg P, McGlathery KJ, Zieman JC (2015) Subtropical seagrass ecosystem metabolism measured by eddy covariance. Mar Ecol Prog Ser 529:75–90

Long MH, Rheuban JE, McCorkle DC, Burdige DJ, Zimmerman RC (2019) Closing the oxygen mass balance in shallow coastal ecosystems. Limnol Oceanogr 64:2694–2708

Long MH, Sutherland K, Wankel SD, Burdige DJ, Zimmerman RC (2020) Ebullition of oxygen from seagrasses under supersaturated conditions. Limnol Oceanogr 65: 314–324

McDowell RE, Amsler MO, Li Q, Lancaster JR Jr, Amsler CD (2015) The immediate wound-induced oxidative burst of *Saccharina latissima* depends on light via photosynthetic electron transport. J Phycol 51:431–441

Miller GW, Morgan CA, Kieber DJ, King DW and others (2005) Hydrogen peroxide method intercomparision study in seawater. Mar Chem 97:4–13

Millero FJ, Sotolongo S (1989) The oxidation of Fe(II) with H_2O_2 in seawater. Geochim Cosmochim Acta 53: 1867–1873

Moffett JW, Zafiriou OC (1990) An investigation of hydrogen peroxide chemistry in surface waters of Vineyard Sound with $H_2{}^{18}O_2$ and $^{18}O_2$. Limnol Oceanogr 35:1221–1229

Moffett JW, Zafiriou OC (1993) The photochemical decomposition of hydrogen peroxide in surface waters of the eastern Caribbean and Orinoco River. J Geophys Res Oceans 98:2307–2313

Moffett JW, Zika RG (1987) Reaction kinetics of hydrogen peroxide with copper and iron in seawater. Environ Sci Technol 21:804–810

Novak AB, Pelletier MC, Colarusso P, Simpson J and others (2020) Factors influencing carbon stocks and accumulation rates in eelgrass meadows across New England, USA. Estuar Coast 43:2076–2091

Olsen JL, Rouzé P, Verhelst B, Lin YC and others (2016) The genome of the seagrass *Zostera marina* reveals angiosperm adaptation to the sea. Nature 530:331–335

Orth RJ, Carruthers TJB, Dennison WC, Duarte CM and others (2006) A global crisis for seagrass ecosystems. Bioscience 56:987–996

O'Sullivan DW, Neale PJ, Coffin RB, Boyd TJ, Osburn CL (2005) Photochemical production of hydrogen peroxide and methylhydroperoxide in coastal waters. Mar Chem 97:14–33

Pei Y, Wang Z, Yan W, Zhou B (2024) Characterization of ascorbate-glutathione cycle response in *Zostera marina* seedlings under short-term temperature surge. Front Mar Sci 11:1390074

Petasne RG, Zika RG (1997) Hydrogen peroxide lifetimes in south Florida coastal and offshore waters. Mar Chem 56: 215–225

Peyer SM, Maricle BR, Young DR (2020) Effect of sulfide and the role of root mass on metabolic fluxes in the seagrass *Zostera marina.* Environ Exp Bot 180:104267

Piao MJ, Kang HK, Yoo ES, Koh YS, Kim DS, Lee NH, Hyun JW (2012) Photo-protective effect of *Polysiphonia morrowii* Harvey against ultraviolet B radiation-induced keratinocyte damage. J Korean Soc Appl Biol Chem 55: 149–158

Price D, Worsfold PJ, Fauzi R, Mantoura C (1994) Determination of hydrogen peroxide in sea water by flow-injection analysis with chemiluminescence detection. Anal Chim Acta 298:121–128

Punitha T, Phang SM, Juan JC, Beardall J (2018) Environmental control of vanadium haloperoxidases and halocarbon emissions in macroalgae. Mar Biotechnol 20:282–303

Rasmusson LM, Lauritano C, Procaccini G, Gullström M, Buapet P, Björk M (2017) Respiratory oxygen consumption in the seagrass *Zostera marina* varies on a diel basis and is partly affected by light. Mar Biol 164:140

Rose AL, Webb EA, Waite TD, Moffett JW (2008) Measurement and implications of nonphotochemically generated superoxide in the equatorial Pacific Ocean. Environ Sci Technol 42:2387–2393

Ross C, Alstyne KLV (2007) Intraspecific variation in stress-induced hydrogen peroxide scavenging by the ulvoid macroalga *Ulva lactuca*. J Phycol 43:466–474

Ross C, Küpper FC, Vreeland V, Herbert Waite J, Jacobs RS (2005) Evidence of a latent oxidative burst in relation to wound repair in the giant unicellular chlorophyte *Dasycladus vermicularis*. J Phycol 41:531–541

Satoh Y, Wada S, Hisamatsu S (2019) Seasonal variations in iodine concentrations in a brown alga (*Ecklonia cava* Kjellman) and a seagrass (*Zostera marina* L.) in the northwestern Pacific coast of central Japan. J Oceanogr 75: 111–117

Sewelam N, Jaspert N, Van Der Kelen K, Tognetti VB and others (2014) Spatial H_2O_2 signaling specificity: H_2O_2 from chloroplasts and peroxisomes modulates the plant transcriptome differentially. Mol Plant 7:1191–1210

Shaked Y, Armoza-Zvuloni R (2013) Dynamics of hydrogen peroxide in a coral reef: sources and sinks: H_2O_2 dynamics in a coral reef. J Geophys Res Biogeosci 118:1793–1801

Short FT, Polidoro B, Livingstone SR, Carpenter KE and others (2011) Extinction risk assessment of the world's seagrass species. Biol Conserv 144:1961–1971

Stabenau E, Zepp R, Bartels E, Zika R (2004) Role of the seagrass *Thalassia testudinum* as a source of chromophoric dissolved organic matter in coastal south Florida. Mar Ecol Prog Ser 282:59–72

Sutherland KM, Coe A, Gast RJ, Plummer S and others (2019) Extracellular superoxide production by key microbes in the global ocean. Limnol Oceanogr 64:2679–2693

Sutherland KM, Wankel SD, Hansel CM (2020) Dark biological superoxide production as a significant flux and sink of marine dissolved oxygen. Proc Natl Acad Sci USA 117: 3433–3439

Sutherland KM, Grabb KC, Karolewski JS, Taenzer L, Hansel CM, Wankel SD (2021) The redox fate of hydrogen peroxide in the marine water column. Limnol Oceanogr 66: 3828–3841

Tcherkez G, Farquhar GD (2007) On the $^{16}O/^{18}O$ isotope effect associated with photosynthetic O_2 production. Funct Plant Biol 34:1049–1052

Twigg IM, Baltar F, Hall JR, Hepburn CD (2020) Revealing hydrogen peroxide as an external stressor in macrophyte-dominated coastal ecosystems. Oecologia 193: 583–591

Valdez SR, Zhang YS, van der Heide T, Vanderklift MA, Tarquinio F, Orth RJ, Silliman BR (2020) Positive ecological interactions and the success of seagrass restoration. Front Mar Sci 7:91

Wang F, Lv Y, Lin L, Xu N, Lu K, Sun X (2018) Characterization of a respiratory burst oxidase homolog from *Gracilariopsis lemaneiformis* (Rhodophyta) during stress and phytohormone treatments. Bot Mar 61:511–519

Waycott M, Collier C, McMahon K, Ralph P, McKenzie L, Udy J, Grech A (2019) Vulnerability of seagrasses in the Great Barrier Reef to climate change. In: Climate change and the Great Barrier Reef: a vulnerability assessment. The Great Barrier Reef Marine Park Authority and Australian Greenhouse Office, p 193–236

Weinberg I, Bahlmann E, Michaelis W, Seifert R (2013) Determination of fluxes and isotopic composition of halocarbons from seagrass meadows using a dynamic flux chamber. Atmos Environ 73:34–40

Winterbourn CC (1995) Toxicity of iron and hydrogen peroxide: the Fenton reaction. Toxicol Lett 82–83:969–974

Wuttig K, Heller MI, Croot PL (2013) Pathways of superoxide (O_2^-) decay in the eastern tropical North Atlantic. Environ Sci Technol 47:10249–10256

Yan W, Wang Z, Pei Y, Zhou B (2024) Adaptive responses of eelgrass (*Zostera marina* L.) to ocean warming and acidification. Plant Physiol Biochem 206:108257

Yuan J, Shiller AM (2001) The distribution of hydrogen peroxide in the southern and central Atlantic Ocean. Deep Sea Res II 48:2947–2970

Zafiriou OC (1990) Chemistry of superoxide ion-radical (O_2^-) in seawater. I. $pK^{\cdot}_{asw}$ (HOO) and uncatalyzed dismutation kinetics studied by pulse radiolysis. Mar Chem 30:31–43

Zamocky M, Furtmuller PG, Obinger C (2008) Evolution of catalases from bacteria to humans. Antiox Redox Signal 10:1527–1548

Zang Y, Liu J, Tang XX, Zhou B (2018) Description of a *Zostera marina* catalase gene involved in responses to temperature stress. PeerJ 6:e4532

Zhang Y, Zhao P, Yue S, Liu M and others (2021) New insights into physiological effects of anoxia under darkness on the iconic seagrass *Zostera marina* based on a combined analysis of transcriptomics and metabolomics. Sci Total Environ 768:144717

Editorial responsibility: Erik Kristensen, Odense, Denmark
Reviewed by: P. Croot and 2 anonymous referees

Submitted: May 28, 2024
Accepted: November 8, 2024
Proofs received from author(s): December 30, 2024